LIMNOLOGY
and
OCEANOGRAPHY: METHODS

Limnol. Oceanogr.: Methods 8, 2010, 1–15

The application of holography to the analysis of size and settling velocity of suspended cohesive sediments

*George W. Graham and W. Alex M. Nimmo Smith**
University of Plymouth, Plymouth, U.K.

Abstract

Suspended cohesive sediments commonly occur in flocculated form. The flocculation process significantly increases particle size, settling velocity, and settling flux in comparison to unflocculated particles. To better understand suspended particles, a new instrument for in situ imaging using digital inline holography is presented and evaluated. With a resolution of 7.4 µm per pixel and a field of view of 7.4 × 7.4 mm, the instrument generates sharply focused images of particles from approximately 20 µm to 7 mm in diameter at up to 25 frames per second. A significant advantage of holography over current imaging systems is that in-focus images are obtained over a substantial depth of field. Contained in small-diameter cylindrical housings, the instrument presents minimal flow disruption and is easily deployable. Digitally recorded holograms are reconstructed and analyzed for number and size of particles in a fully automated manner. To assess the systems' potential, particle size distributions for two grades of quartz sand are compared with those from a laser diffraction particle sizer and are found to exhibit good similarity. To simultaneously estimate particle size and settling velocity, a modification to the system is demonstrated in which settling particles are automatically tracked and sized. The resulting relationships between settling velocity and effective density as functions of particle size are characteristic of suspended cohesive sediments and empirical power-law descriptors of these relationships show excellent agreement with previously published studies.

The majority of fine-grained suspended sediments across the entire fluvial to marine continuum occur in flocculated form, i.e., as aggregates composed of smaller constituent components. Understanding the behavior of flocculated particles is of fundamental importance in the comprehension of the dynamics of cohesive suspensions because the process of aggregate formation significantly changes the size and settling speed of aggregates, and thus the mass settling flux, in comparison with single particle settling. The flocculation process is also important to the capture, transport, and release of waterborne contaminants and pathogens because these can bind to, and be incorporated within, aggregates that grow or are disaggregated during flocculation and de-flocculation. Suspended particle size, as well as the mass of sediment in suspension, also has implications for the propagation of optical and acoustic signals through water masses. To characterize dynamically active cohesive suspensions, methods for observing the temporal variation in particle size distribution are required. Large, flocculated aggregates are notoriously fragile and can be easily disrupted during sampling so non-intrusive in situ particle size measurements that cause minimal disruption to the sampling volume are desirable.

A number of indirect methods of estimating particle size have been developed that use small angle laser scattering to estimate particle size (e.g., Bale and Morris 1991), with the most commonly adopted commercial package being Laser In Situ Scattering and Transmisometery (LISST) systems (Agrawal and Pottsmith 2000, 2004). Such techniques use scattering theory for regularly shaped spherical particles to invert small angle laser scattering to particle size. Unless the shape and optical scattering characteristics of suspended natural particles are known a priori, systems that depend solely on the measurement of diffraction angles may be prone to error when distinctly nonspherical particles are present. To address some of these issues, a plethora of direct observation methods have also been developed principally using still photography (Eisma et al. 1990; Benson and French 2007) or videography. Video-based methods are capable of simultaneous size and settling velocity measurement and such instruments include INSSEV (Fennessy et al. 1994; Manning and Dyer 1999), INSSECT (Mikkelsen et al. 2004), and DIPSTICK (Kim and Sandford 2007). The addition of particle settling velocity measurement is beneficial because this parameter is widely used in the calculation of carbon fluxes to the ocean floor as well as in many

*Corresponding author: E-mail: animmosmith@plymouth.ac.uk

sedimentological and engineering applications in environmental science and waste water engineering. Focal plane photographic systems generally rely on high magnification lenses to achieve good resolution of the small particles in suspension (typically micron to millimeter scale) at the expense of the field of view and the depth of field. As a consequence, total sampling volume sizes can be extremely small, and therefore, the total number of in-focus imaged objects is reduced. Further limitations of such systems are associated with the potential of particle size bias introduced by measuring particles at the limits of the depth of field (which are therefore out of focus), and long processing times since measurements of particles from still images are conventionally analyzed manually. Recently, there has been a drive toward automation, with some investigators developing semi-automated methods (Fox et al. 2004) or real-time size and tracking algorithms (Kim and Sandford 2007).

Holography is a proven method that can offer complete solution to the limitations of focal plane photography in imaging small objects. It is becoming increasingly used to image and measure oceanic particles and microorganisms (Katz et al. 1999; Malkiel et al. 1999; Owen and Zozulya 2000; Sheng et al. 2006; Sun et al. 2007, 2008), but there has been limited research into the dynamics of cohesive sediments with holographic systems (c.f., Black et al. 2001; Sun et al. 2002; Perkins et al. 2004; Sun et al. 2004). In this paper, we present a novel compact and submersible system (developed at the University of Plymouth) that uses digital in-line holography to obtain synoptic particle size, shape, and number concentration of suspended particles. We also present details of modifications to this system, which enable the simultaneous measurement of both size and settling velocity of suspended particulates in a fully automated manner. Such measurements allow the estimation of effective densities for individual particles and the determination of settling flux distributions.

Materials and procedures

A hologram (Fig. 1) is the recording of the interference pattern that results from the interaction between two beams of coherent light derived from 1) a collimated source and 2) diffraction and/or refraction of the source beam by objects present in the path (Fig. 2A illustrates the optical setup used in this paper). The fringes around the objects in the image contain both the phase and amplitude information of the diffracted wave that can be used to deduce the size and position of the scattering object relative to the imaging plane. In classical holography, to reconstruct an image collimated light is reapplied to the hologram, which acts as a diffraction grating, generating the original object beam that appears to diverge from object positions behind the hologram thus creating a virtual image. To view objects recorded in a digital hologram, the classical reconstruction process (the diffraction of coherent light by hologram) is simulated numerically so that the object beam wave fronts can be reconstructed on a plane at

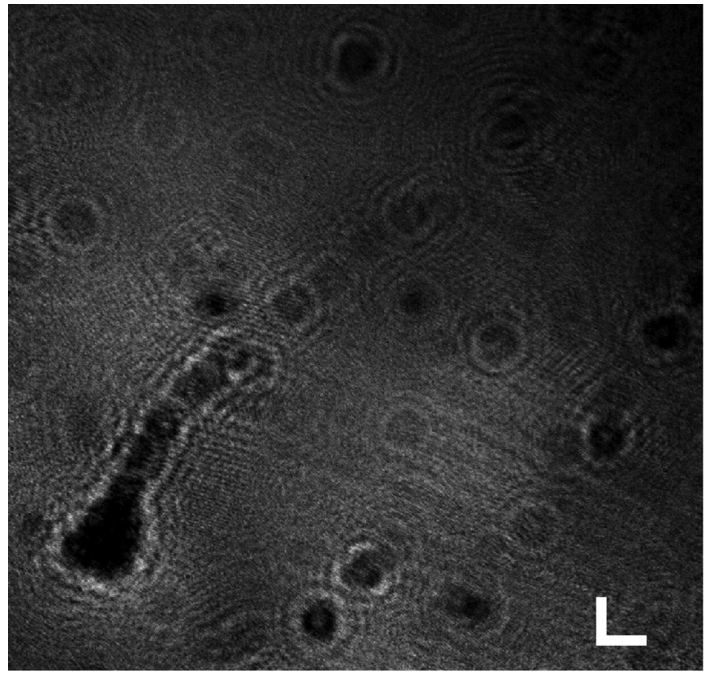

Fig. 1. 2-D intensity distribution of digital in-line hologram captured by the charged-coupled device within the Submersible Digital Holographic Particle Imager described in this article. The scale bar in the lower right corner is 250 μm in length.

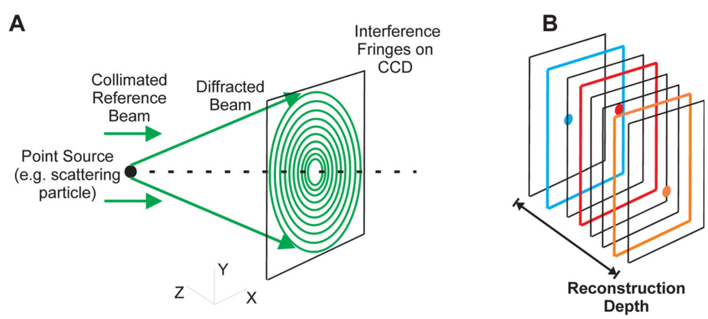

Fig. 2. Schematic of (A) in-line hologram generation by interference between collimated reference beam and diffracted beam from a scattering source and (B) transformation of 2-D hologram image to 3-D volume with in-focus objects (colored blobs) occupying discrete planes within the sampling volume.

any distance from the recording plane (Fig. 2B). Consequently, the significant advantage of holography is that focus does not have to be fixed a priori since any object within the sampling volume can be bought into focus during the reconstruction process. This benefit also means that it is possible to image microscopic objects within larger sampling volumes than has been possible with conventional photography or videography.

Submersible digital holographic particle imager—The submersible system is shown in Fig. 3A and a schematic of the optical setup for digital in-line holography is presented in Fig. 3B. The optical system is contained within two 100 mm

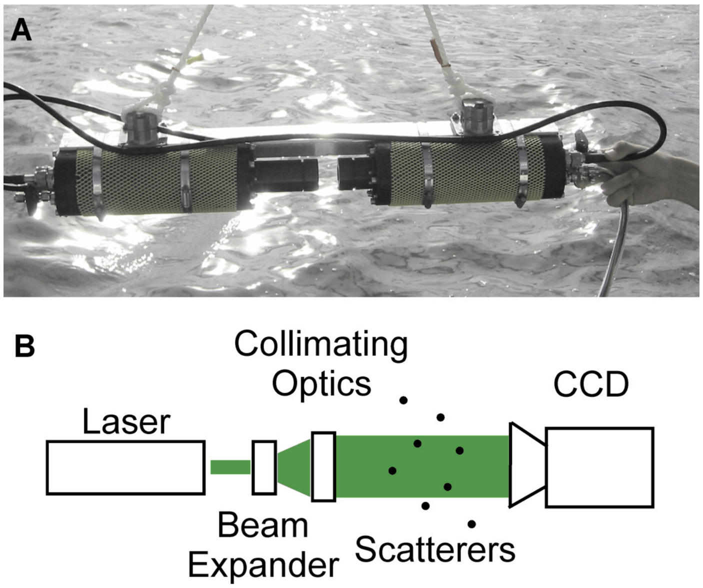

Fig. 3. Illustration of Submersible Digital Holographic Particle Imager before in situ deployment (A). A schematic diagram of the optical setup relating to 3(A) is shown in (B).

diameter aluminum tubes. A 532 nm, 80 mW continuous wave laser-diode and collimating optics are contained in the left housing. A pair of small diameter extension tubes pass the collimated beam from the left housing to the right. The sampling volume occupies the space between the extension tubes, and as objects pass through the volume, they diffract the laser beam. The resulting interference pattern (or fringe) is imaged by a charged-coupled device (CCD) (1002 × 1004 pixels, 7.4 µm per pixel, 1 MB per image) in the right housing at up to 25 frames per second. The separation of each housing by the small diameter extension tubes minimizes flow interference of the camera and laser housings with the sampling volume. Blur-free images are recorded by modulating the laser and triggering the camera to obtain a 10-µ*s* exposure, allowing measurements in relative flows of up to 0.5 m s^{-1}.

Images are not magnified so the resolution is that of the CCD, the pixel size of which has been independently calibrated against a standard stage micrometer. The housings can be moved horizontally on a bar to vary the separation between the ends of the extension tubes and thus the horizontal extent of the sampling volume depending upon the concentration of particles in suspension. With a nominal separation of 30 mm between the extension tubes, the sampling volume is 1.653 cm^3. A third housing (not shown) contains the PC104-based control electronics and data storage. The submersible system is tethered to the surface for power as well as interactive control with data download by LAN connection. The system can also be configured for autonomous deployment.

Holographic reconstruction—We reconstruct the captured in-line holograms digitally, using a simplification of the convolution approach (Schnars and Jüeptner 1994; Schnars and Jüeptner 2005) presented by Owen and Zozulya (2000). This simplification allows us to do the reconstruction without assumptions concerning particle size and proximity to the CCD as would be required if we were to use a Fresnel transformation. We are also able to remove the DC component of the reference beam. Using the 2-D intensity distribution of an individual hologram captured by the CCD, we use linear filtering to reconstruct, at any depth (z) across the sample volume, a plane slice of the sample volume. For computational efficiency, this filtering, and recovery of the final image, is performed in Fourier space using a combination of Fast Fourier Transforms (FFT) and inverse FFTs across all z within the sampling volume.

Analysis of particle characteristics—Once the 2-D intensity image $[U(x,y)]$ has been reconstructed into a 3-D volume $[I_z(x,y;1{:}N)]$, where N represents the maximum number of reconstruction planes, we must locate all objects within the volume, bring each into focus, and then calculate size and shape statistics for them.

Particle detection—The approximate x,y positions of all objects within the reconstructed volume are found by collapsing the reconstructed volume to a single plane $[I_{collapse}(x,y)]$ in order to make all in-focus particles visible. Since diffracting objects within the sampling volume cause large changes in intensity over the depth of the sampling volume, and intensity is largely uniform through the volume where objects are absent, we assign each pixel of the collapsed image the standard deviation (σ) measured over the entire depth to generate a 2-D map of object location:

$$I_{collapse}(x,y) = \sigma[I_z(x,y;1:N)] \qquad (1)$$

To remove speckle noise, we median filter $I_{collapse}(x,y)$ with a 3×3 pixel kernel. A histogram shape-based thresholding approach to segmentation (Otsu 1979) allows the approximate 2-D location and size (via a pixel count) for all objects in the sampling volume to be determined. To further eliminate noise, a Region of Interest (ROI) is defined around the 2-D position of any object in $I_{collapse}(x,y)$ comprised of ≥ 20 pixels. This object size threshold is arbitrarily selected as separating objects with discernable shape from those that appear as diffuse point sources. A collapsed image and superimposed ROI is illustrated in Fig. 4A. The ROI is extended across all reconstruction planes in $I_z(x,y;1{:}N)$ to generate a Volume of Interest (VOI):

$$I_{VOI}(x_{ROI}, y_{ROI}, 1:N) = I_z(x_{ROI}, y_{ROI}; 1:N) \qquad (2)$$

where x_{ROI} and y_{ROI} are the 2-D x and y extents of the ROI respectively. Once VOIs are determined for all objects in the field of view, which meet the size criteria of ≥ 20 pixels, all subsequent processing steps are performed on these segments of the full hologram reconstruction. Using segments rather than the full reconstructed volume (which requires at least a factor of 20 times more storage space than the original 2-D image) increases efficiency in computations, memory usage, and data storage.

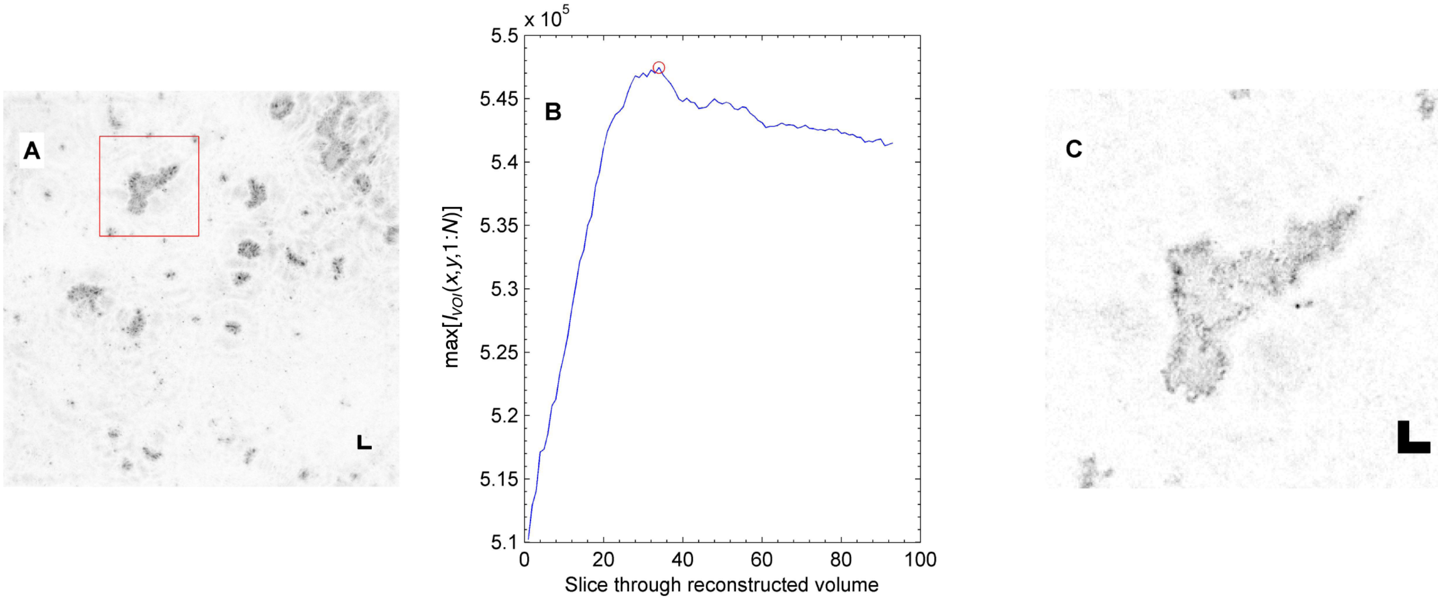

Fig. 4. (A) Illustration of full field of view of the collapsed image [$I_{collapse}(x,y)$] generated from Fig. 1 with ROI (red box) generated around an object of interest (scale bar indicates 250 µm). (B) Illustrates variation of the focus metric (Eq. 3) through the planes of the VOI, the position of z_{focus} is indicated with a red circle. (C) shows the in-focus plane of the object within the VOI [$I_{VOI}(x_{ROI},y_{ROI},z_{focus})$] with a scale bar indicating 150 µm.

Particle autofocusing—To accurately estimate object size and shape, a sharply focused image of the object is required. A range of sophisticated focusing metrics have been developed (Malkiel et al. 2003; Burns and Watson 2007), but we have opted to use a fast yet simple method to determine the plane of maximal focus within each object's VOI. The maximum in the VOI intensity as a function of depth through the VOI is determined and used to indicate the position of maximum focus:

$$I_{focus}(x_{ROI}, y_{ROI}, z_{focus}) \tag{3}$$

where $z_{focus} = max\left\{\sum_{1}^{i}\sum_{1}^{j}[I_{VOI}(x_{ROI}, y_{ROI}, 1:N)]\right\}$ and the indices i and j are equal to the length of the ROI in the x and y directions, respectively.

Although this method is not fully immune to false maxima generated by noise, our experience has shown that this simple method is fast and extremely reliable for autofocusing objects within reconstructed volumes (Fig. 4B,C).

Particle segmentation and sizing—Because holography is diffraction dominated, in-focus images of objects (refer to Fig. 4C) tend to exhibit strong edges and a dark-side edge detection method (Benson and French 2007) is used to segment individual objects within their ROI. Thresholding on these ROI subdomains takes very little computational effort in comparison with global thresholds applied to the whole field of view. However, since the interior of objects have lower intensities than their edges, such thresholding methods tend to "fracture" visually coherent particles into multiple connected component pixels. A sequence of steps illustrated in Fig. 5 compensates for the thresholding artifacts and enables the number of pixels comprising the 2-D projected area of the object to be estimated.

Natural, suspended particles often have very complicated shapes spanning the entire continuum from small, compact, and approximately spherical individual grains through to complex, loosely connected multi-cored aggregations with fractal-like geometry and crenulated perimeters (Fig. 6 and images in Manning and Dyer [2002] and Maggi et al. [2006]). The definition of particle size is clearly problematic due to the irregular morphologies exhibited by suspended particles (Droppo et al. 2005). We opt for a Euclidean shape equivalent size, using the number of pixels in an object's flood-filled convex hull (A) to determine the diameter of a sphere D_{convex} with equivalent projected area:

$$D_{convex} = \sqrt{\frac{4A}{\pi}} \tag{4}$$

Note that although we accurately locate the in-focus plane for any object, the exact extent of the object in the z dimension (i.e., the size of the object in the third dimension) cannot be accurately determined due to uncertainties introduced by recording resolution (as illustrated by Sheng et al. (2006)). In addition, an extremely large number of closely spaced reconstruction planes through the object would be required to identify the limits of the object. Such measurements are considered too computationally expensive for our present purposes and are not considered further in this paper.

Modifications for simultaneous size and settling velocity estimation—The vertical settling velocity of particles suspended in the water column is an important characteristic because it determines the vertical flux of mass through the water column and

Fig. 5. Image-processing sequence performed on individual object within an ROI. An in-focus object (A) undergoes segmentation by edge detection (B). The strong edges of the object are highlighted by multiply connected pixels. Morphological closure and de-noising are performed (C) before a convex hull is fitted (D) and flood filled (E). The scale bar in A is 250 μm in length.

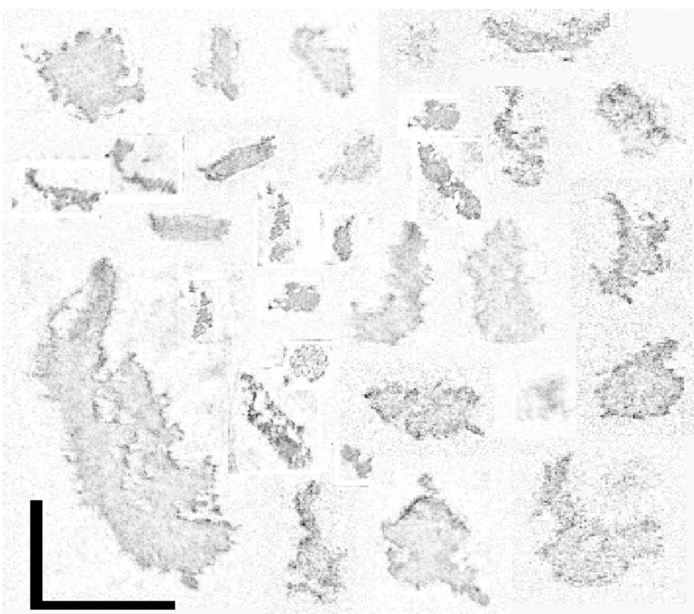

Fig. 6. In-focus gray-scale images, chosen at random from a number of holograms to illustrate salient characteristics of (typically flocculated) particles. Notice the distinctly nonspherical nature of these particles. Scale bar in lower left is 250 μm in length.

has a direct bearing on deposition rates and the removal of chemical elements from suspension. Because cohesive sediments can flocculate into aggregates containing both mineral and biological material that are both larger and more porous than their constituent parts, the density of such particles can vary greatly and can be significantly less than a solid particle of the same size due to the presence of interstitial water within the floc (Hill et al. 1998; Fox et al. 2004). Due to the stochastic nature of the flocculation process and the inclusion of different quantities and types of mineral and organic matter within a floc matrix, it is impossible to accurately predict in situ floc settling velocities or densities from a measured size since these quantities can exhibit considerable variance for a given particle size.

A simultaneous measurement of both particle size and settling velocity can be used to estimate aggregate density and determine a settling flux. Numerous submersible apparatus have been developed for in situ or quasi in situ determination of both particle size and settling velocity either relying upon time-lapse photography or videography (*see* Dyer et al. [1996] and Mantovanelli and Ridd [2006] for reviews). The limitations of optical systems with a small depth of focus have already been discussed, and in this section, we extend the benefits of our submersible holographic imaging system to the simultaneous estimation of particle size and settling velocity. One of the first applications of holography to size and settling velocity determination was by Carder (1979). Carder et al. (1982) developed a free-floating sediment trap equipped with a submersible holographic particle velocimeter using 35 mm holographic film. Data analysis was manually conducted resulting in size, settling velocity, and density estimates for a small number of particles ($n = 11$). Costello et al. (1989) used a similar design for extended deployments, acquiring approximately 4000 holograms. Most recently, van Hout and Katz (2004) developed a laboratory based digital in-line holographic system to estimate the density of pollen grains settling in water. We shall demonstrate the method that we have developed to estimate aggregate density and determine the settling flux for a cohesive suspension in a fully automated manner.

Hardware—Laboratory adaptations of the Submersible Holographic Particle Imager (developed at the University of Plymouth) for the determination of particle settling velocity are illustrated in Fig. 7. A settling column with internal dimensions of 100 × 100 × 190 mm and sapphire glass optical windows (40 mm diameter) located with their center lines 75 mm above the bed of the column is positioned between the extension tubes of the Holographic Particle Imager housings. The separation between the extension tubes is 134 mm result-

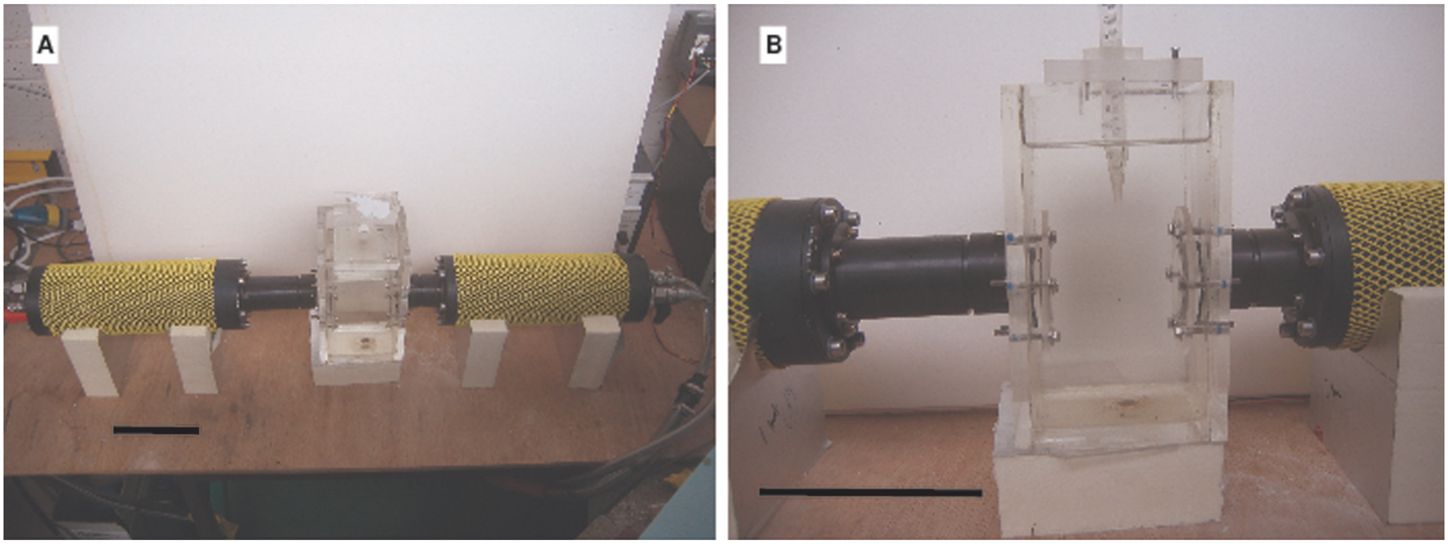

Fig. 7. Submersible Digital Holographic Particle Imager modified for ex situ sampling with laboratory settling column (A) and close-up of settling column and particle delivery by pipette inserted into top of settling column (B). For scale, the black bar in each image is 100 mm in length.

ing in a usable sampling volume of 7.4 cm^3. The settling column is filled with saline water and cohesive particles are withdrawn from a pre-made suspension of natural intertidal mud (90:10 mineral:organic mass from mudflats of the Tamar Estuary, U.K.) by pipette and allowed to settle vertically within the settling column in a similar manner to Gratiot and Manning (2004), Graham and Manning (2007), and Manning et al. (2007). The Digital Holographic Particle Imaging system samples at 10 frames per second, sufficient to capture particles settling at speed of up to 17 mm s^{-1}. A positive density difference of $\Delta\rho_w$ = 3.4 kg m^{-3} is maintained between the column water and the source suspension to minimize the impact of schlieren on the holographic imaging and to reduce buoyancy effects on the settling velocity of flocculated particles.

Particle tracking software—The work flow for automated particle sizing and tracking is illustrated in Fig. 8. Given inputs of a raw hologram timestack and some user-defined processing parameters (which include variables such as the number of frames to process and the number of reconstruction planes to use) the linked processes in region A of Fig. 8 perform the numerical reconstruction, particle detection, autofocusing, and sizing of each object within each hologram as has previously been discussed for the in situ system. The processes in region B of Fig. 8 control the formation of trajectories for each of the automatically detected particles in the timestack of holograms. For any particle in the first hologram of the timestack, possible matches to particles in the second hologram are identified using logic statements to ensure 1) similarity in projected area and major axis dimensions, 2) that the centroid of candidate particles are below that of the initial particle (i.e., candidates are settling vertically), and 3) that horizontal displacement is within user-defined limits. To find the best match between candidates and the initial particle, 2-D gray-scale cross-correlation of the in-focus images of the initial and candidate particles is performed. Since individual frames in time stacks are separated by 0.1 s, calculating the frame-to-frame displacements between the initial particle and its best match in a subsequent frame results in a frame pair settling velocity. This frame pair tracking procedure is iterated over all particles and all frame-pairs within the time stack. Trajectories are formed by linking the size, shape, and position metrics of each particle that can be successfully tracked over at least 4 sequential frames. Automated quality control of these trajectories is performed using logic to remove trajectories that contain gradients in particle position that exceed user defined limits. Region C of Fig. 8 is an optional step that utilizes a GUI for manual quality control of particle trajectories. An example of a particle trajectory that results from this automated sequence of particle tracking (regions A-C in Fig. 8) is presented in Fig. 9. The final stage in the automated system is the analysis of particle trajectories and the calculation of trajectory averaged quantities and their variance (Region D of Fig. 8). These calculations are described in the following section.

Processing procedure—Following Fennessy et al. (1994), two corrections are applied to the raw, instantaneous settling velocity obtained from frame-pair displacements of each particle. First compensation for the wall drag induced by the settling column is applied (Allen 1985). Second, the ambient settling velocity (i.e., settling velocity in source waters of lower salinity) is calculated. Using a modified Stokes formula (Eq. 5), instantaneous effective (or excess) density in relation to the settling column water is derived for each independent particle realization:

$$\rho_e = \rho_f - \rho_w = \frac{(W_s 1.03)18\mu}{D_{convex}^2 g} \quad (5)$$

where W_s is particle settling velocity, μ is kinematic viscosity, g the acceleration due to gravity, and ρ_f and ρ_w the density of

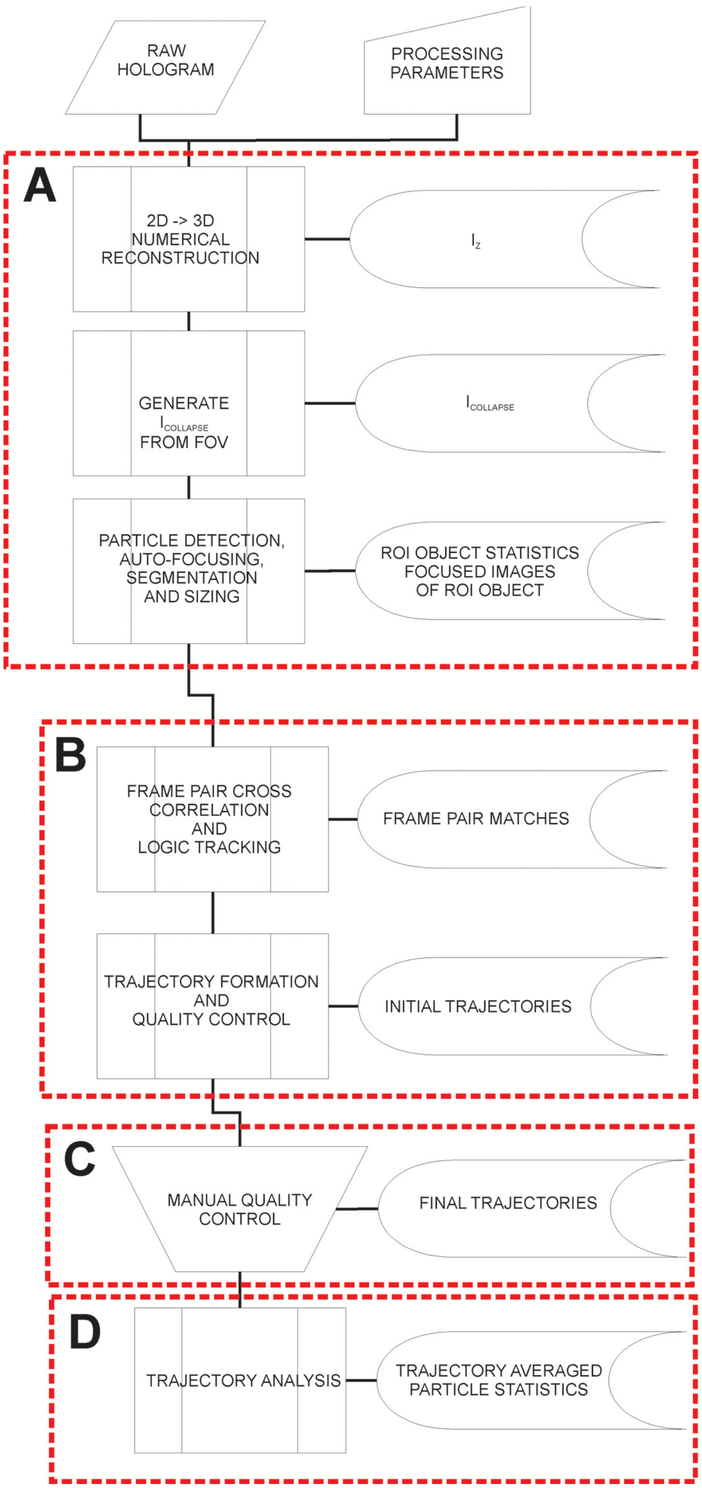

Fig. 8. Process flow diagram illustrating particle-tracking sequence. The sequence can be subdivided into 4 discrete units (A-C, flowing vertically with processes indicated by rectangles and intermediate stored outputs also indicated). For description, *see* the main text.

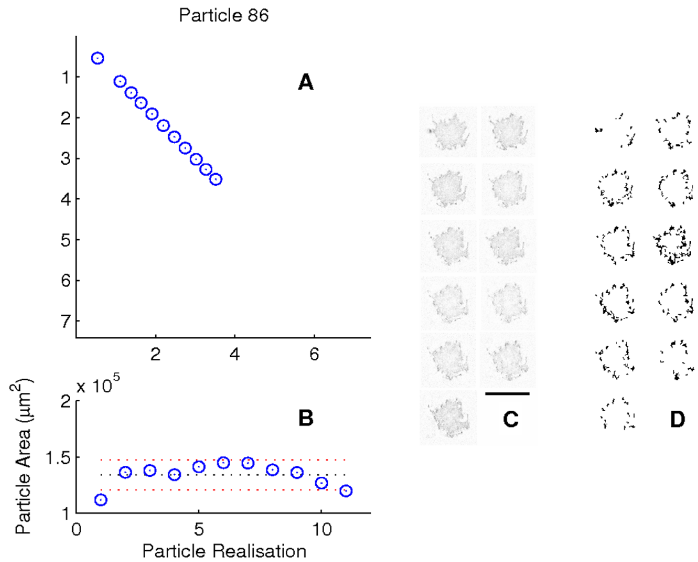

Fig. 9. Graphical illustration of particle tracking. A single particle is tracked over 11 sequential frames (A) from left to right across the field of view (7.44 × 7.44 mm). From each particle realization, statistics such as the projected area (B, blue circles) are derived. The black dashed line in B is the trajectory averaged particle area and the red-dashed lines illustrate .10% of this mean. The individual gray-scale realizations of the particle are shown in C (the scale bar is 500 µm in length) and the results after segmentation, but before particle area is in filled by the convex hull fitting operation, are shown in D.

floc and water, respectively. The ambient effective density of each particle (the effective density in the source water) is derived from knowledge of the density difference between the source waters ($\Delta\rho_w$) and the density of the water in the settling column:

$$\rho_{e\,ambient} = \rho_{e\,column} - \Delta\rho_w \tag{6}$$

The instantaneous settling velocity is then adjusted using Stokes equation with the calculated instantaneous ambient effective density from Eq. 6 to obtain the instantaneous ambient settling velocity:

$$W_{s\,ambient} = \frac{D_{convex}^2 \rho_{e\,ambient}\, g}{18\mu} \tag{7}$$

The ambient-settling velocity is always marginally higher than the raw-settling velocity (provided that the settling column salinity is higher than ambient). Eq. 7 is considered valid for particles with Reynolds numbers up to 0.5. Where this is exceeded, the Oseen Modification (Ten Brinke 1994) is used and results in a slight increase in effective density. The modification takes the form:

$$\rho_{e\,Oseen} = \rho_{e\,ambient}\left(1 + 0.1875 R_e\right) \tag{8}$$

with the particle Reynolds number given by

$$R_e = \frac{\rho_w W_{s\,ambient} D_{convex}}{\mu} \tag{9}$$

Assuming the mean dry density of mineral and organic components of a flocculated particle (ρ_{mo}) is equal to 2256 kg

m^{-2}, the dry mass of a flocculated particle can be determined as:

$$M_{dry} = \left(\frac{\pi D_{convex}^3}{6}\right)\left[\frac{\rho_e \rho_{mo}}{(\rho_{mo} - \rho_w)}\right] \qquad (10)$$

Summation over the entire sample results in a total mass concentration which, with knowledge of the volume of water extracted from the source suspension by pipette, can be converted to a suspension concentration (mass per unit volume). The product of suspension concentration and trajectory averaged settling velocity per particle followed by summation over the entire sample generates a mass settling flux for the entire population of settling particles. Such flux calculation methods are well accepted and have been previously applied by Syvitski et al. (1995), Sternberg et al. (1999), and Mikkelsen et al. (2004).

Assessment

To validate the accuracy of the size measurements obtained from the Digital Holographic Particle Imager, we have conducted a laboratory comparison with a Malvern Instruments Hydro 2000G, which uses low angle laser scattering to estimate particle size. Since the response of laser diffraction to significantly nonspherical particles is uncertain (van Wijngaarden and Roberti 2002), for this comparison we use two grades of well-weathered beach sands (Teignmouth, Devon, U.K.) to examine similarity in the particle size distributions generated by the two instruments. Sands were graded by sieving into a coarse fraction (nominally 500–710 µm) and a fine fraction (nominally 125–180 µm) through nested sieves for 15 min (Folk 1980). For analysis, both fractions were pre-wetted and analyzed in the Hydro 2000G without ultrasonic aggregation or the addition of de-flocculant prior to sampling. For analysis with the Digital Holographic Particle Imager, a water-filled glass cuvette was placed between the extension tubes so that pre-wetted samples could be gravitationally settled through the laser beam in the laboratory.

Fig. 10 illustrates the size distribution comparisons. For the fine sediment samples (Fig. 10A), there is a good agreement between the modal peak (210.2 µm) in the particle size distribution by volume (PSD) generated by the Digital Holographic Particle Imager and the Hydro 2000G. For both systems, the modal peak in particle size is significantly greater than the nominal sieved range of sizes and suggests that particles orient themselves during sieving with longest axes normal to the sieve mesh such that "coarse" particles are able to propagate through the stack and are captured on finer meshes. The width of the distributions are similar in the region 125–420 µm, but the Digital Holographic Particle Imager exhibits a pronounced left-skew with more small particles by volume in the range 11.5–125 µm than the Hydro 2000G. The secondary mode in the Digital Holographic Particle Imager PSD at 356 µm is generated by overlapping particles, the diffraction pattern of which is interpreted as a single large particle. The same process can be seen to influence

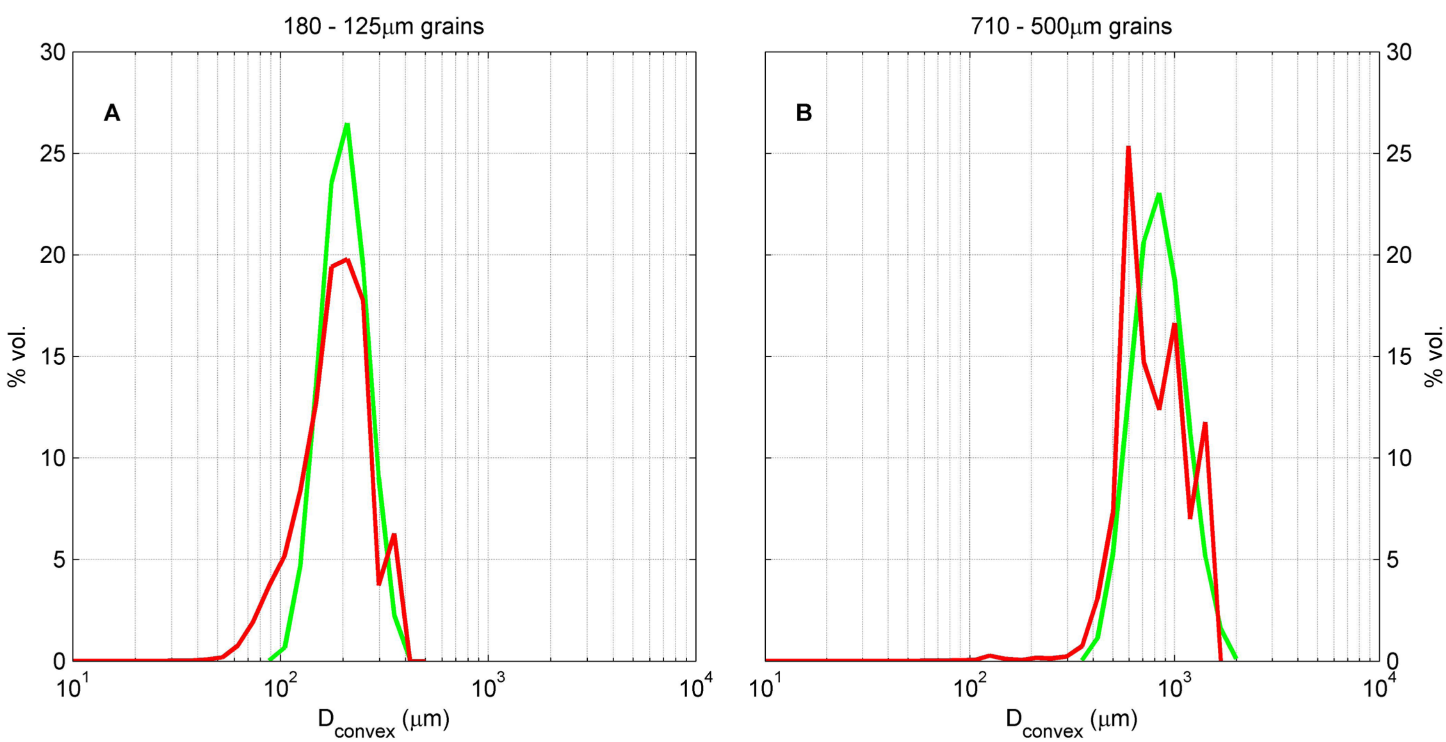

Fig. 10. Comparison of Particle Size Distributions from Holographic Particle Imager (red line) and Malvern Hydro 2000G laser sizer (green line) for fine (A) and coarse (B) quartz sands. Particle size data are binned into 27 logarithmically spaced bins over the interval 10–1000 µm.

the PSD from the Digital Holographic Particle Imager for the coarse fraction (Fig. 10B) at 1000 and 1414 µm. Interestingly, in this coarse fraction comparison, the widths of the PSDs are almost identical in the range 353–1682 µm and, as in Fig. 10A, the Digital Holographic Particle Imager is left skewed by very small particles but the principal modes are separated by almost 250 µm. Possible explanations for this discrepancy are discussed in the following section.

Fig. 11 illustrates the trajectory averaged settling velocity and effective density data generated by our automated analysis software from a population of settling aggregates during a single settling experiment taken from a series of experiments conducted by Graham (2008) using natural intertidal cohesive sediments. The population of 647 particles has been segregated on the basis of size into micro flocs (83.3% by number) and macroflocs (16.7%) based on the distinction proposed by Manning (2001). Because we obtain several independent realizations of each particle over a time stack of frames, it is possible to estimate the variability in characteristic metrics over a particles trajectory in addition to calculating trajectory averaged metrics for size, settling velocity, and effective density. Trajectory averaged sizes range from 30.07 (±1.64) – 443.05 (±3.41) µm while settling velocities (Fig. 11A) range from 0.10 (±0.02) – 5.73 (±2.34) mm s^{-1}, and effective densities (Fig. 11B) range from 11.49 (±1.81) – 1435.9 (±47.33) kg m^{-3}. Settling velocities increase with particle size while effective densities are inversely related to particle size; that is, larger particles settle quickly but they have a loosely bound, "fluffy" structure incorporating interstitial pore spaces in comparison to slow settling but more compact smaller particles. The relationships between particle size and settling velocity or effective density can be well described by a power law, indicating that the settling particles approximate natural fractal objects (i.e., they exhibit pseudo-fractal behavior, or self-similarity, over the limited range of observable scales). The sample is dominated by small particles which will play an important role in optical and acoustic scattering. The large particles, although less than 20% of the sample by number, dominate the distribution by volume and in combination with their fast settling velocities make significant contributions (>90%) to the total mass settling flux as illustrated in Fig. 12. In Fig. 13, power law relations for settling velocity and effective density as functions of particle size obtained from a number of published studies are contrasted with power law relations fitted to averaged data from 5 settling experiments conducted by Graham (2008) using the holographic system discussed in this paper. There is clearly large variability in observed particle size, settling velocity, and effective density within and between the studies presented in Fig. 13 as well as the rates of change in settling velocity or effective density as a function of particle size. It is clear however that the relationships of positive and negative correlations between settling velocity and effective density as functions of particle size, illustrated in Fig. 11, are characteristic of flocculated, cohesive sediments in general. In addition, data derived using the Digital Holographic Particle Imager lies in the midst of the scattered, general relationships for settling velocity and effective density reported in the literature.

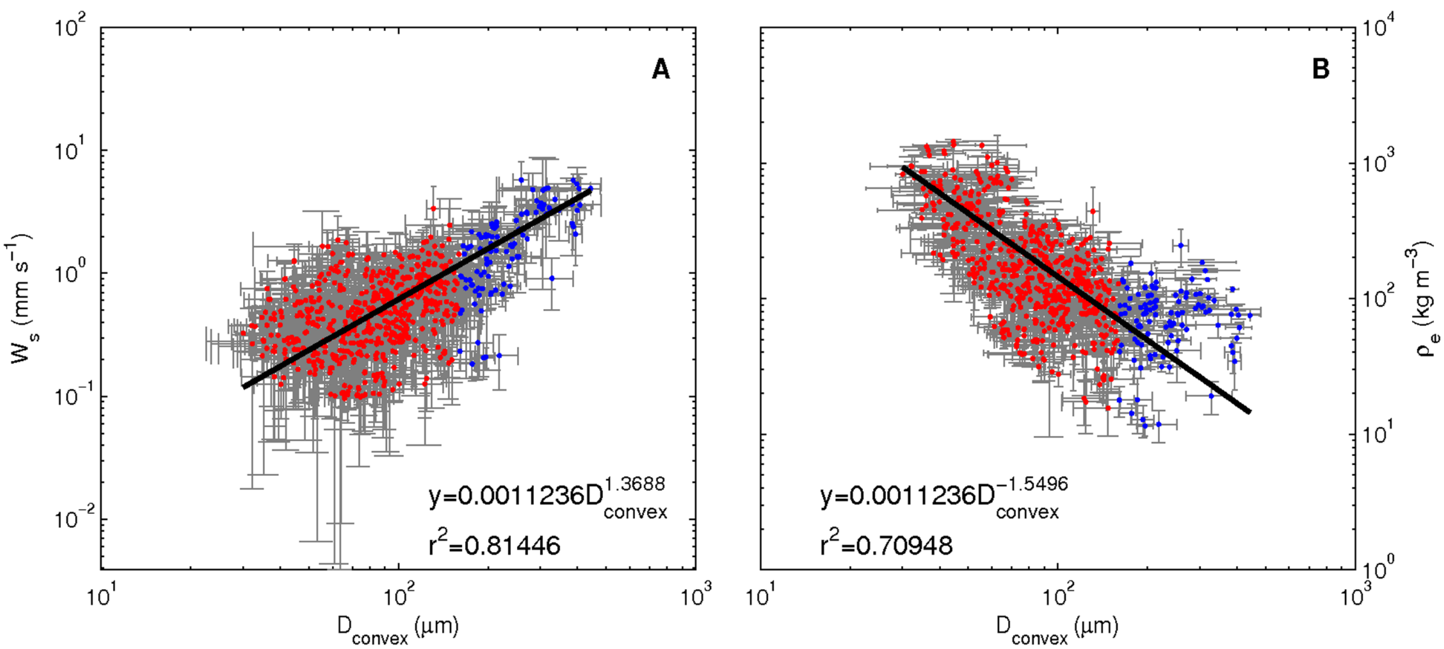

Fig. 11. Trajectory averaged settling velocity (A) and effective density (B) as functions of spherical equivalent particle size. Solid dark line indicates least squares fit of power law. Error bars are 1 standard deviation around trajectory averaged quantities. Red coloration indicates microflocs (D ≤ 160 µm), and blue coloration indicates macroflocs (D > 160 µm).

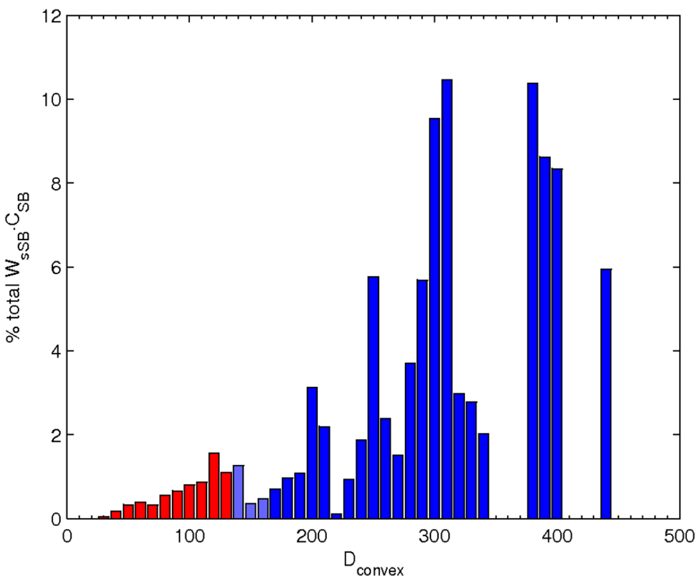

Fig. 12. Contributions to the total settling flux (defined as the product of the size band averaged settling velocity and suspension concentration) from each particle size band. Red coloration indicates microflocs (D ≤ 160 µm), and blue coloration indicates macroflocs (D > 160 µm). Although few by number, macroflocs contribute 91% of the total mass settling flux.

Discussion

A number of systems currently exist for the in situ determination of particle size. We have chosen to develop a holographic system because holography has the advantage of enabling the focusing of objects within a large sampling volume to produce crisp images of the suspended particles from which size and shape metrics can be determined.

A range of parameters to represent particle size have previously been adopted, for example Fennessy (1994) used a single dimensional linear characteristic length (horizontal axis length) and Manning and Dyer (1999) use both horizontal and vertical axes to derive a square equivalent size. We choose the spherical equivalent size since we will be reporting, in future publications, on the comparison between the Digital Holographic Imager and existing laser sizing instrumentation that make spherical assumptions in their size estimation. An important assumption of representing particle size by the equivalent spherical diameter method is that the projected area is equivalent to the equatorial area (πr^2), i.e., the 2-D projection of the object is assumed to be a slice directly through the object's central plane. With the holographic system, we are able to generate sharply focused images of individual particles, and we assume that the position of maximal focus results in a slice through the particle's central plane.

The comparison between the Digital Holographic Imager and the Malvern Hydo 2000G particle size distributions (Fig. 10) is extremely encouraging because there is generally excellent agreement between the two systems. It is important to remember that the size distributions from the Hydro 2000G are automatically averaged over many realizations whereas the size distribution from the Holographic Imager is essentially a single realization. For the fine fraction (Fig. 10A), the modal peaks of particle size distributions for both systems are in exact agreement. The apparent discrepancy between the percentage of total volume occupied by modal particle size results from the observation by the Digital Holographic Particle Imager of both finer and apparently coarser particles than measured by the Hydro 2000G. Of interest is the secondary mode in the size distribution from the Digital Holographic Particle Imager which occurs at 365 µm in Fig. 10A (and can also be seen at 1000 and 1414 µm in Fig. 10B). These features are produced from the occasional overlapping sand grains within a hologram, which our automated software interprets as a single grain. The projected areas, and thus spherical equivalent size and volume of overlapping grains, are significantly larger than individual nonoverlapping grains and generate highly peaked secondary and tertiary modes in the particle size distribution. To lessen the influence of overlapping grains on size distributions generated by the Digital Holographic Particle Imager, we are currently developing a method to isolate the individual overlapping particles and estimate their sizes.

The Holographic Imager sees a larger proportion of the total volume in the fine tail of the distribution in Fig. 10A (and to a lesser extent in Fig. 10B) than the Hydro 2000G. We postulate that this is a consequence of the differences in sample volume and dispersion methods used by the two systems as well as in the actual sediment sample that analysis was conducted on. The Hydro 2000G wet sample dispersion unit has an approximate volume of 1 L and a pumped system that recirculates suspended particulates at high speed through the laser sampling volume. The laboratory setup for the Digital Holographic Imager used a small water-filled cuvette into which particles were dropped from a spatula and imaged as they settled. Although the sediment samples were pre-wetted and manually homogenized before size analysis with either instrument, it is impossible to ensure that the samples input to each system have exactly the same proportions of particle sizes. Because it was impossible to image exactly the same population of suspended particles for both systems, it is not surprising that there are small differences between particle size distributions, especially in the fine tails of the distributions. The particle size distributions for the coarse fraction (Fig. 10B) exhibit a difference in the modal particle size of some 250 µm. Such differences may be associated with the discrepancies between the two systems already discussed. In addition, size estimates from the Hydro 2000G may also be influenced by preferential hydrodynamic orientation of suspended particles while they are pumped through the laser beam, presenting their longest axis to the sensor array (Gabas et al. 1994), and overlapping of coarse particles, which we have noted can strongly influence the shape of the size distribution derived using the

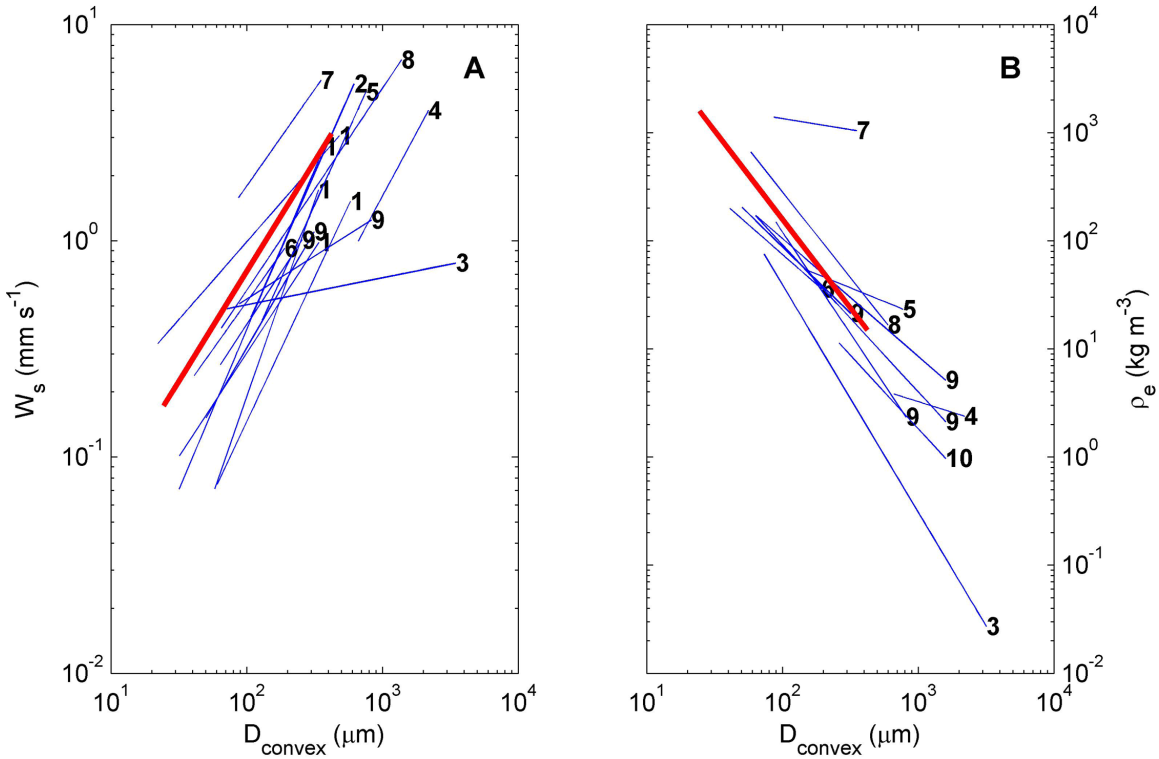

Fig. 13. Comparison of power law relations for size and settling velocity (A) and size and effective density (B) derived in previous studies (blue lines) with those derived using the holographic system presented in this paper (red lines). Numbered lines refer to the studies of 1) Fennessy et al. (1994), 2) van Leussen and Cornelisse (1993), 3) Syvitski et al. (1995), 4) Hill et al. (1998), 5) Sternberg et al. (1999), 6) Manning and Dyer (1999), 7) van der Lee (2000), 8) Fox et al. (2004), 9) Graham and Manning (2007), and 10) Curran et al. (2007).

Digital Holographic Particle Imager. Particle shape effects may be responsible for the discrepancies in the modal peak of the coarse sample between the Holographic Imager and the Hydro 2000G. The fine sand sample may be sufficiently small so as to be "seen" as spherical, which results in good agreement between the two instruments. As previously discussed, it is impossible to be certain, even for approximately regularly shaped particles, how laser diffraction size estimates respond to particle shape without having simultaneous angular scattering measurements and images of the particle that cause the scattering. Kelly et al. (2006) argue that laser diffraction data are a combination of particle breadth, longest dimension, and other particle dimensional measurements as particle shape becomes increasingly complex. Further improvements in agreement between the size distributions for the two systems for near-spherical particles may be achieved by averaging multiple subsamples from the Digital Holographic Particle Imager to smooth replicate-to-replicate variability.

Having a system that generates images of the particles is a major benefit over instruments that use low angle laser scattering alone to infer particle size, especially when working with natural (i.e., non spherical) and cohesive sediments. Fig. 1 illustrates the interference pattern generated by a complex flocculated aggregate consisting of a prominent "head" (in the lower left of the image) and a long tail comprising smaller aggregates bound together by clear threads (possibly extra cellular polymeric substances excreted by microorganisms) extending across the field of view (to the top right corner of the image). Fig. 4C illustrates a flocculated particle that appears to have a "ragged" perimeter. Fig. 6 illustrates a range of particles that exhibit large variation in size, shape, and perimeter irregularity. The response of laser-scattering instruments to such particles is, at present, an unknown. Gabas et al. (1994) and Kelly et al. (2006) have shown that for non-spherical particles, the interpretation of the diffraction events occurring from each of the chords that can be drawn across the cross-sectional area projection of a particle does not lead to a single description of particle size. Flocs may be "seen" as multiple-sized scatterers if the work of Karp-Boss et al. (2007) on plankton can be extended, by analogy, to flocculated particles. Aggregates may give a size peak associated with an imaginary spheroid that encompasses the aggregate as a whole and secondary peaks associated with imaginary spheroids that encompass smaller subcomponents of the floc. Large aggregates do not consist of solid materials and as a consequence, light may be diffracted through pores within the aggregate, which will contribute to the diffraction pattern in a similar way as isolated smaller particles would. The perimeter of a floc may be the major contributor of diffraction, but it is impossible to discount the secondary contributions that may occur from smaller component parts and pore space, which may alias derived size estimates to smaller size bins (van Wijngaarden and Roberti 2002) and cause the appearance of "ghost" particles (Thonon et al. 2005) in laser diffraction measurements. Although the effects of small departures from nonsphericity on laser diffraction measurements can be accounted for (Agrawal et al. 2008), there is still much to be discovered about the influence of flocculated aggregates upon laser diffraction measurements. The benefit of an imaging system such as the Submersible Digital Holographic Particle Imager, which we have presented in this paper, is that an in-focus image of a particle is generated from which functional light-scattering units can be assessed, and all subcomponents of complex, flocculated particles can be included in the particle size and shape estimates.

At present, we use a combination of different image segmentation algorithms to threshold images of complex aggregates before estimating their sizes. As previously noted, this leads to the fragmentation of particles, and we approximate the particles' true projected area with a convex hull. This procedure is effective for particles such as those illustrated in Fig. 4C and 5A but tends to reduce long stringy particles to their components parts. Breaking the functional unit of a floc up into subcomponents in this manner may not be overly problematic when considering the light-scattering properties of these aggregates, because it is the small component parts that dominate the scattering characteristics of flocs. However, such fragmentation leads to misrepresentation of true particle size, poor estimate of particle density and significant errors in the distribution of mass settling flux over the spectrum of measured particle sizes. Thonon et al. (2005) have shown that densities of apparently small particles can be over-estimated because they appear as single particles falling very rapidly, whereas they are actually contained within larger aggregates (of low density) that settle, as a functional unit, very quickly. At present, we are working on improvements to our current thresholding methodology to overcome the limitations of particle thresholding, but we are aware that it is probably unreasonable to expect any automated method to reliably segment such complicated flocculated particles as that illustrated in Fig. 4A and some compromise between full automation/processing speed and the accurate segmentation of all particles is unavoidable.

The relationship between particle settling velocity, effective density and particle size as illustrated in Figs. 11 A and B can be considered characteristic of suspended cohesive sediments across a wide range of environments since they are consistent with the trends illustrated in Fig. 13 which contrasts power law relations from a number of published studies. Flocculated particles can be envisaged as fractal entities whose structure, as particle size increases, becomes increasingly porous resulting in an inverse relation between effective density and particle size. The power law fit to the averaged results of 5 laboratory settling experiments which we have obtained with the Digital Holographic Particle Imager lies in the midst of the parameter space defined by previous studies. The variability in range of particle sizes, settling velocities, and effective densities between the studies with which we compare our method can be attributed to variations in suspended particulate matter concentration, shear stress, and biological mediation that contribute to the flocculation process. Differences in the range of particle sizes and settling velocities observed may also be influenced by the sampling methods used. Our observed particle sizes range over an order of magnitude from 30.07 (±1.64) – 443.05 (±3.41) µm, which is similar to size ranges observed with estuarine muds by Fennessy et al. (1994), Manning and Dyer (1999), and Graham and Manning (2007). There is conflicting evidence relating to the effect of pipetting, the method that we use to transfer flocculated particles from their source suspension to the settling column, on the observed floc size distributions. Gibbs (1982) has shown that for small (≤70 µm) mineral flocs, subsampling by pipetting has no significant effect on floc sizes. However, Eisma et al. (1991) showed large discrepancies between in situ particle size distributions and those after Owen tube recovery and Coulter Counter/pipette analysis. Manning and Dyer (1999) have postulated that pipette sampling has a negative impact on floc size and structure, but discrepancies between in situ and ex situ size distributions are more likely to be associated with sample collection, transport, and handling protocols (e.g., Owen tube sampling or bottling water samples) since Gratiot and Manning (2004) have shown that use of a wide bore pipette method creates minimal floc disruption during sample acquisition. Despite using a wide bore pipette for floc sampling, we cannot guarantee that the sampling process is completely nondestructive, but the close agreement between our settling velocity and effective density data and the reported relationships with particle size from other studies (Fig. 13) suggests that, if there is floc disruption occurring during sampling, it has little impact and would be masked by naturally occurring variability in the flocculation process. The general agreement between studies illustrated in Fig. 13 gives us confidence that the Submersible Digital Holographic Particle Imager causes little floc disruption and adequately resolves particle size and settling velocity over previously observed ranges. Although sampling by pipette has allowed us to demonstrate our particle sizing and tracking methodology, we have some questions about how representative such a sampling strategy is. We are therefore in the process of developing the holographic system for the simultaneous acquisition of particle size and settling velocity data from cohesive suspensions in situ in a fully automated manner. We will report on these developments in future publications.

Laboratory adaptation of the Submersible Holographic Imager to include a settling column has enabled us to demonstrate the amalgamation of holographic particle imaging and particle tracking in order to estimate particle settling velocities, effective densities, and mass settling fluxes for cohesive suspensions. There have been several attempts to use holography to simultaneously measure size and settling velocity of suspended particles in the oceanic environment (Carder 1979; Carder et al. 1982; Payne et al. 1984; Costello et al. 1989), but such studies have generally been limited to a small number of imaged particles because data processing has been conducted manually. Developments in digital holography, data storage, and computational power have enabled us to develop a fully automated method to size and track many hundreds of particles during a single settling experiment in a highly reliable manner. Combining the advantages of digital in-line holography, automated particle sizing and tracking, and the algorithms of Fennessy et al. (1994) has resulted in a powerful method for the determination of size, settling velocity, effective density, and the settling flux of cohesive suspensions. Multiple realizations of an individual particle as it settles through the field of view (e.g., Fig. 9) enable variability in particle size and settling velocity to be propagated through the processing methodology to generate error estimates for the ambient settling velocity, effective density, and other derived quantities. Figs. 11A and 11B illustrate floc settling velocity and effective density as functions of particle size. Until now, such figures have rarely been presented with any estimate of the errors associated with these quantities. Four small particles in Fig. 11A have large standard deviations in the calculated settling velocities. These errors in the ambient settling velocity are associated with small variations in the instantaneous settling velocity and binary representation of the particle from which the projected area is estimated. Once the error in these two terms are propagated through calculations for effective density and ambient settling velocity, the uncertainty in the ambient settling velocity can be of the same order of magnitude as the settling velocity itself. We have left these particles in Figs. 11A and 11B because they illustrate the importance of accurately estimating the projected area of particles. This is especially important for small particles for which even small percentage changes in their binary representation result in large projected area variations.

Conclusions

We have presented a submersible digital in-line holographic particle imaging system, which we are currently using to measure the size of suspended particles in coastal waters. The instrument has a resolution of 7.4 µm per pixel with a field of view of 7.4 × 7.4 mm and is capable of imaging particles from approximately 20 µm to 7 mm. The major advantage with a holographic system is that it is possible to image particles over a substantial depth of field and then focus each particle after acquisition to obtain sharp images of the particles from which to estimate size. The digital reconstruction and particle sizing is conducted in a fully automated manner with minimal user intervention. Particle size distributions for quartz sand closely resemble those obtained with a Malvern Hydro 2000G low angle laser diffraction sizing instrument. There are some slight discrepancies associated with differences in sample delivery, dispersion, and replication, but the similarities are encouraging. Multiple overlapping particles are problematic for any imaging system and cause false secondary maxima in particle size distributions. Using information on the distribution of particles through the sampling volume, which is unique to holographic systems, we are investigating methods to identify overlapping particles and size the individual grains to reduce these discrepancies. The major benefits of imaging systems are obvious when dealing with suspensions of irregularly shaped particles or flocculated aggregates within cohesive suspensions. Since the light-scattering properties of such particles cannot be known a priori, determining their size from laser diffraction may prove to be problematic. Obtaining focused images of the particles enables size estimates to be generated without recourse to assumptions concerning particle shape. All imaging systems rely heavily upon the accurate characterization of imaged particles in binary form. We are currently making further improvements to the segmentation methods that the Digital Holographic Particle Imager utilizes to refine our size estimates and make it possible to accurately characterize particle shape.

Since cohesive sediments are acutely sensitive to hydrodynamic conditions, there is no consistent relationship between particle size and settling velocity. This makes estimation of settling fluxes from particle size information alone prone to error. We have presented a “proof-of-concept” laboratory adaptation of the submersible particle-imaging system, which enables us to simultaneously measure particle size and settling velocity of cohesive sediments. Using multiple realizations of each particle as it settles allows us to generate trajectory averaged size and settling velocities and attribute error terms to these estimates. This information can then be used to calculate effective densities for the particles and settling fluxes for the entire sample. Settling velocity and effective density variations with particle size show consistency with previously published studies from a range of marine environments. A significant benefit over previous instruments for size and settling velocity estimation is that the Digital Holographic Particle Imager makes use of fully automated particle tracking, which enables us to size and track many hundreds of particles per settling experiment in a reliable and repeatable manner. Encouraged by our initial laboratory tests, we are in the process of developing a system for the in situ determination of particle size and settling velocity. We are also exploring distributed computing and GPU parallel processing as future avenues from which it would be possible to gain significant decreases in computational time associated with the reconstruction of digital holograms.

Such a fully automated system would bring increased ease and speed to the collection and analysis of particle size, shape, and settling velocity data across a range of environments from the laboratory to marine, freshwater, and engineered systems.

References

Agrawal, Y., and H. Pottsmith. 2000. Instruments for particle size and settling velocity observations in sediment transport. Mar. Geol. 168:89-114.

——— and ———. 2004. LISST laser diffraction sensors advance sediment monitoring. Sea Technol. 45:33-38.

———, A. Whitmire, O. Mikkelsen, and H. Pottsmith. 2008. Light scattering by random shaped particles and consequences on measuring suspended sediments by laser diffraction. J. Geophys. Res. 113:C04023.

Allen, J. 1985. Principles of physical sedimentology. Allen & Unwin.

Bale, A., and A. Morris. 1991. In situ size measurments of suspended particles in estuarine and coastal waters using lazer diffraction, p. 197-208. *In* J. Syvitski [ed.], Principles, methods, and applications of particle size analysis. Cambridge Univ. Press.

Benson, T., and J. French. 2007. InSiPID: A new low-cost instrument for in situ particle size measurement in estuarine and coastal waters. J. Sea Res. 58(3):167-188.

Black, K., H. Sun, G. Craig, D. Paterson, J. Watson, and T. Tolhurst. 2001. Incipient erosion of biostabilised sediments using particle-field optical holography. Environ. Sci. Technol. 35(11):2275-2281.

Burns, N., and J. Watson. 2007. Data extraction from underwater holograms of marine organisms. *In* Oceans 2007 - Europe. Institute of Electrical and Electronics Engineers (IEEE): [doi: 10.1109/OCEANSE.2007.4302407].

Carder, K. 1979. Holographic microvelocimeter for use in studying ocean particle dynamics. Opt. Engineer. 18(5):524-525.

———, R. Steward, and P. Betzer. 1982. In situ holographic measurements of the sizes and settling rates of oceanic particulates. J. Geophys. Res. 87(C8):5681-5685.

Costello, D. K., K. L. Carder, P. R. Betzer, and R. W. Young. 1989. In situ holographic imaging of settling particles: Applications for individual particle dynamics and oceanic flux measurements. Deep Sea Res. A 36(10):1595-1605.

Curran, K., P. Hill, T. Milligan, O. Mikkelsen, B. Law, X. Durrieu de Madron, and F. Bourrin. 2007. Settling velocity, effective density, and mass composition of suspended sediment in a coastal bottom boundary layer, Gulf of Lions, France. Cont. Shelf Res. 27:1408-1421.

Droppo, I. G., G. G. Leppard, S. N. Liss, and T. G. Milligan. 2005. Opportunities, needs, and strategic direction for research on flocculation in natural and engineered systems, p. 407-421. *In* I. G. Droppo, G. G. Leppard, S. N. Liss, and T. G. Milligan [eds.], Flocculation in natural and engineered systems. CRC Press.

Dyer, K., and others. 1996. A comparison of in situ techniques for estuarine floc settling velocity measurements. J. Sea Res. 36(1/2):15-29.

Eisma, D., and others. 1990. A camera and image-analysis system for in situ observation of flocs in natural waters. Neth, J. Sea Res. 27:43-56.

———, P. Bernard, G. Cadee, V. Ittekkot, and J. Kalf. 1991. Suspended matter particle size in some West-European estuaries; Part I: Particle size distribution. Neth. J. Sea Res. 28(3):193-214.

Fennessy, M. 1994. Development and testing of an instrument to measure estuarine floc size and settling velocity in situ. Ph.D. thesis, University of Plymouth.

———, K. R. Dyer, and D. Huntley. 1994. INSSEV: an instrument to measure the size and settling velocity of flocs in situ. Mar. Geol. 117:107-117.

Folk, R. 1980. Petrology of sedimentary rocks. Hemphill Publishing.

Fox, J., P. Hill, T. Milligan, A. Ogston, and A. Boldrin. 2004. Floc fraction in the waters of the Po River prodelta. Cont. Shelf Res. 24:1699-1715.

Gabas, N., L. Hiquily, and C. Laguuerie. 1994. Response of laser diffraction particle sizer to anisometric particles. Part. Part. Syst. Character. 11(2):121-126.

Gibbs, R. J. 1982. Effect of pipetting on mineral flocs. Environ. Sci. Technol. 16:119-121.

Graham, G. 2008. Biomediation of turbulence and suspended sediment characteristics in marsh surface flows: The influence of *Spartina anglica*. Ph.D. thesis, University of Plymouth.

———, and A. Manning. 2007. Floc size and settling velocity within a *Spartina anglica* canopy. Cont. Shelf Res. 27(8):1060-1079.

Gratiot, N., and A. Manning. 2004. An experimental investigation of floc characteristics in a diffusive turbulent flow. *In* Ciavola, P., and M.B. Collins [eds.], Sediment transport in European estuaries. J. Coast. Res. Special Issue 41:105-113.

Hill, P. S., J. P. Syvitski, E. Cowan, and R. Powell. 1998. In situ observations of floc settling velocities in Glacier Bay, Alaska. Mar. Geol. 145:85-94.

Karp-Boss, L., L. Zazavedo, and E. Boss. 2007. LISST-100 measurements of phytoplankton size distribution: Evaluation of the effects of cell shape. Limnol. Oceanogr. Methods 5:396-406.

Katz, J., P. Donaghay, J. Zhang, S. King, and K. Russel. 1999. Submersible holocamera for detection of particle characteristics and motions in the ocean. Deep Sea Res. I 46:1455-1481.

Kelly, R., K. DiSante, E. Stranzl, J. Kazanjian, P. Bowen, T. Matsuyama, and N. Gabas. 2006. Graphical comparison of image analysis and laser diffraction particle size analysis data obtained from the measurements of non-spherical particle systems. AAPS PharmSciTech 7(3):E1-E14.

Kim, Y., and P. Sandford. 2007. Variability of grain size, settling velocity and effective density of suspended particles in the Chesapeake Bay turbidity maximum. *In* Proceedings of

INTERCOH-2007. Brest (France): Ifremer. p. 113-114. The conference was held by Ifremer.

Maggi, F., O. Alquaddoomi, and J. Katz. 1999. Measurements of plankton distribution in the ocean using submersible holography. Measure. Sci. Technol. 10:1142-1152.

———, A. J. Manning, and J. C. Winterwerp. 2006. Image separation and gemoetric characterisation of mud flocs. J. Hydrol. 326:325-348.

Malkiel, E., J. Abras, and J. Katz. 2003. Automated scanning and measurements of particle distributions within a holographic reconstructed volume. Measure. Sci. Technol. 15:601-612.

Manning, A. 2001. A study of the effect of turbulence on the properties of flocculated mud. Ph.D. thesis, University of Plymouth.

———, and K. Dyer. 1999. A laboratory examination of floc characteristics with regard to turbulent shearing. Mar. Geol. 160:147-170.

——— and ———. 2002. The use of optics for the in situ determination of flocculated mud characteristics. J. Optics A: Pure and Applied Optics 4:571-581.

———, P. Friend, N. Prowse, and C. Amos. 2007. Estuarine mud flocculation properties determined using an annular mini-flume and the labsfloc system. Cont. Shelf Res. 27(8):1080-1095.

Mantovanelli, A., and P. Ridd. 2006. Devices to measure settling velocities of cohesive sediment aggregates: A review of the in situ technology. J. Sea Res. 56(3):199-226.

Mikkelsen, O., T. Milligan, P. Hill, and D. Moffatt. 2004. INSSECT - an instrumented platform for investigating floc properties close to the bed. Limnol. Oceanogr. Methods 2:226-236.

Otsu, N. 1979. A threshold selection method from gray-level histograms. IEEE Trans Sys Man Cyber 9(1):62-66.

Owen, R., and A. Zozulya. 2000. In-line digital holographic sensor for monitoring and characterizing marine particulates. Opt. Eng. 39:2187-2197.

Payne, P., K. L. Carder, and R. Steward. 1984. Image analysis techniques for holograms of dynamic ocean particles. Appl. Opt. 23(2):204-210.

Perkins, R., H. Sun, J. Watson, M. Player, G. Gust, and D. Paterson. 2004. In-line laser holography and video analysis of eroded floc from engineered and estuarine sediments. Environ. Sci. Technol. 38:4640-4648.

Schnars, U., and W. Jüeptner. 1994. Direct recording of holograms by a CCD target and numerical reconstruction. Appl. Opt. 33(2):179-181.

——— and ———. 2005. Digital holography: Digital hologram recording, numerical reconstruction, and related techniques. Springer.

Sheng, J., E. Malkiel, and J. Katz. 2006. Digital holographic microscope for measuring three-dimensional particle distributions and motions. Appl. Opt. 45(16):3893-3901.

Sternberg, R., I. Berhane, and A. Ogston. 1999. Measurement of size and settling velocity of suspended aggregates on the Northern California continental shelf. Mar. Geol. 154:43-53.

Sun, H., H. Dong, M. Player, J. Watson, D. Paterson, and R. Perkins. 2002. In-line digital video holography for the study of erosion processes in sediments. Measure. Sci. Technol. 13:L7-L12.

———, R. Perkins, J. Watson, M. Player, and D. Paterson. 2004. Observations of coastal sediment erosion using in-line holography. J. Opt. A 6:703-710.

———, D. Hendry, M. Player, and J. Watson. 2007. In situ underwater electronic holographic camera for studies of plankton. J. Ocean. Eng. 32(2):373-382.

———, P. Benzie, N. Burns, D. Hendry, M. Player, and J. Watson. 2008. Underwater digital holography for studies of marine plankton. Phil. Trans. Royal Soc. London A 366:1789-1806.

Syvitski, J. P., K. Asprey, and K. LeBlanc. 1995. In situ characteristics of particles settling within a deep-water estuary. Deep Sea Res. 42:223-256.

Ten Brinke, W. 1994. Settling velocities of mud aggregates in the Oosterschelde tidal basin (The Netherlands), determined by a submersible video system. Est. Coast. Shelf Sci. 39:549-564.

Thonon, I., J. Roberti, H. Middelkoop, M. van der Perk, and P. Burrough. 2005. In situ measurements of sediment settling characteristics in floodplains using a LISST-ST. Earth Surf. Proc. Landforms 30:1327-1343.

van der Lee, W. 2000. Temporal variation of floc size and settling velocity in the Dollard estuary. Cont. Shelf Res. 20(12-13):1495-1511.

van Hout, R., and J. Katz. 2004. A method for measuring the density of irregularly shaped biological aerosols such as pollen. J. Aerosol Sci. 35(11):1369-1384.

van Leussen, W., and J. Cornelisse. 1993. The determination of the sizes and settling velocities of estuarine flocs by an underwater video system. Neth. J. Sea Res. 31:231-241.

van Wijngaarden, M., and J. Roberti. 2002. In situ measurement of settling velocity and particle size distribution with the LISST-ST, p. 295-312. *In* J. C. Winterwerp and C. Kranenburg [eds.], Fine sediment dynamics in the marine environment. Elsevier Science.

Submitted 8 April 2009
Revised 20 August 2009
Accepted 5 October 2009